Journal of
Applied Remote Sensing

Modeling evapotranspiration and its partitioning over a semiarid shrub ecosystem from satellite imagery: a multiple validation

Yuting Yang
Russell L. Scott
Songhao Shang

SPIE

Modeling evapotranspiration and its partitioning over a semiarid shrub ecosystem from satellite imagery: a multiple validation

Yuting Yang,[a,b,c] Russell L. Scott,[d] and Songhao Shang[a]
[a]Tsinghua University, Department of Hydraulic Engineering, State Key Laboratory of Hydroscience and Engineering, Beijing 100084, China
yyt08@mails.tsinghua.edu.cn
[b]National Centre for Groundwater Research and Training, Adelaide, South Australia 5001, Australia
[c]Flinders University, School of the Environment, Adelaide, South Australia 5001, Australia
[d]Southwest Watershed Research Center, USDA-ARS, 2000 E. Allen Road., Tucson, Arizona 85719

Abstract. Numerous modeling approaches have been proposed to estimate evapotranspiration (ET) and its partitioning between evaporation from soil (E) and transpiration from vegetation (T) over the last several decades. Although these ET models claimed to give reasonable E and T partitioning, few studies have compared their modeling results with direct E and T observations. In this study, a hybrid dual source scheme and trapezoid framework based evapotranspiration model (HTEM) fed with MODIS data was applied in a Chihuahuan Desert shrubland during the growing season of 2003 and validated with direct ET measurement using the Bowen-ratio technique and T measurement using scaled-up sap-flow measurements. Results show that the HTEM is capable of decomposing the remotely sensed land surface temperature into temperature components (soil and canopy temperatures) and providing accurate E and T estimates. At satellite overpass time, the root-mean-square error (RMSE) of estimated latent heat flux (LE) is 47.7 W/m^2. The agreement between estimated and simulated LE was largely improved when observed net radiation and ground heat flux were used (35.1 W/m^2). At daily scale, the RMSE of estimated daily ET, E, and T are 0.52, 0.36, and 0.41 mm/day, respectively.
 [DOI: 10.1117/1.JRS.7.073495]

Keywords: evapotranspiration; evaporation; transpiration; remote sensing; shrub ecosystem.

Paper 13192 received Jun. 1, 2013; revised manuscript received Sep. 24, 2013; accepted for publication Oct. 1, 2013; published online Oct. 25, 2013.

1 Introduction

Water-limited ecosystems cover ~50% of the global land area,[1] and the exchanges of energy and mass at the soil–vegetation–atmospheric interface and their interactions with hydrology and ecology has long been an important research topic in these regions.[1–3] However, under the context of global change, large-scale changes in vegetation have been observed in these ecosystems, which may potentially alter the local/regional carbon and water cycling and their feedbacks to the climate system.[4–6] Evapotranspiration (ET) is a major component of the terrestrial hydrological cycle (ca. 60% of land precipitation), which controls land-atmosphere feedbacks via modulating the surface energy budget. The two components of ET, evaporation (E) and transpiration (T), reflecting energy and water fluxes, respectively, from soil via nonbiological processes and from vegetation via biological processes, would effectively assist in developing an understanding of the water status and vegetation distribution characteristics of the interested area. As a result, partitioning ET into its component fluxes becomes a key issue in understanding the change of carbon and water cycling under the changing environment.[7,8]

Using a combination of ground-based measurements, such as eddy-covariance systems, Bowen-ratio systems, weighting lysimeters, sap-flow probes, and stable isotopes, reliable ET

0091-3286/2013/$25.00 © 2013 SPIE

and/or E and T partitioning observations can be obtained.[9–12] However, due to the high cost, complexity, and siting requirements, they are not suitable for large-scale and long-period monitoring of land surface ET.[13] Therefore, mathematical modeling in combination with more globally available data from remote sensing becomes an important tool to quantify ET over larger geographic areas and longer periods.[14,15]

There have been nearly 40 years of progress for estimating ET using thermal remote sensing techniques.[14,16] However, most of those remote sensing ET models produce only a total ET flux over the combined surfaces of vegetation and soil.[17–19] This is because the land surface temperature (LST) captured by satellite remote sensing is a composite temperature over heterogeneous surfaces. Such models are often referred to as a single-source model. A single-source model treats the land surface as a uniform layer, which, however, cannot distinguish between evaporation and transpiration. This may lead to considerable modeling errors when being applied to partially vegetated surfaces,[20,21] which is often the case for water-limited ecosystems.

To obtain a more realistic description of energy fluxes over partially vegetated surfaces, efforts have been made to develop two-source models that estimate evaporation and transpiration separately from soil and canopy surfaces.[22–26] A major difficulty in this approach is how to decompose the combined LST into component temperatures (i.e., canopy temperature and soil temperature). In the two-source energy balance (TSEB) model,[22,25] the Priestley-Taylor approximation was adopted to give the first estimation of canopy transpiration and the canopy temperature. In its simplified form, concurrent observations of LST at two substantially different view angles were used to determine component temperatures.[26] In the two-source trapezoid model for evapotranspiration (TTME) recently developed by Long and Singh,[23] soil wetness isolines within a trapezoid space of vegetation index (VI)-LST were used to decompose bulk radiative surface temperature into component temperatures. Yang and Shang[27] improved the TTME model by coupling the trapezoid space with a hybrid dual-source modeling scheme to account for the land surface roughness heterogeneity and physiological effects on surface turbulence transport, which is usually simplified in other triangle or trapezoidal framework based ET models. The improved model, named as the hybrid dual source scheme and trapezoid framework based evapotranspiration model (HTEM), showed reasonable ability in partitioning E and T over farmland ecosystems.

Even though these two-source ET models all claimed to give reasonable E and T partitioning, few studies have compared their modeling results with direct E and T observations. Instead, measurements of the total latent heat flux (e.g., eddy covariance towers and energy balance Bowen ratio systems) are often used to validate models. [22,23,26] A separate validation of E and T is warranted to give a more precise understanding of model performance.

The objective of this study is to provide a comprehensive validation of the HTEM in a semiarid shrub ecosystem, particularly on its ability in E and T partitioning. The reason to choose the HTEM is because of its straightforward logic in separating bulk temperature into component temperatures, while assumptions in other models may result in greater uncertainties. For example, in the TSEB model, different values of the Priestley-Taylor coefficient used may lead to substantially different modeling results.[27,28]

This paper is organized as follows. Section 2 provides the framework and details of the HTEM. The study site and data used are described in Sec. 3. The comparisons between modeling results and observations combined with discussions are given in Sec. 4, followed by conclusions in Sec. 5.

2 Methods

2.1 *HTEM*

2.1.1 *Hybrid dual source scheme*

The hybrid dual source scheme is a mixture of layer approach and patch approach to partition the available energy and to estimate the surface energy fluxes for each component (i.e., soil and vegetation).[29] Net radiation is allocated onto canopy and soil surfaces following Beer's law.

$$R_c = R_n[1 - \exp(-k_c \mathrm{LAI})], \tag{1}$$

$$R_s = R_n[\exp(-k_c \mathrm{LAI})], \tag{2}$$

where k_c is the extinction coefficient of radiation attenuation within the canopy; LAI is leaf area index (m^2/m^2); and R_c, R_s, and R_n are the net radiation for canopy, soil, and the mixed surface, respectively (W/m^2). According to surface radiation balance, R_n is calculated from

$$R_n = (1 - \alpha)S_d + \varepsilon\sigma(\varepsilon_a T_a^4 - \mathrm{LST}^4), \tag{3}$$

where α and ε are albedo and emissivity of the mixed surface; σ is Stefan-Bolzmann constant; ε_a is the atmospheric emissivity, which can be estimated following Brutsaert;[30] LST is the bulk surface land surface temperature and T_a is air temperature (°C); and S_d is the downwelling shortwave radiation (W/m^2), which is estimated following Allen et al.[31]

Then, a patch approach is used to partition available energy into the latent heat, sensible heat, and ground heat fluxes.

$$R_c = F_c \times (\mathrm{LE}_c + H_c), \tag{4}$$

$$R_s - G = (1 - F_c) \times (\mathrm{LE}_s + H_s), \tag{5}$$

where H is sensible heat flux, G is ground heat flux, and LE is latent heat flux (W/m^2); substitutes s and c stand for soil and canopy component, respectively. F_c is the fractional vegetation coverage and can be deduced from remotely sensed normalized difference vegetation index (NDVI).

$$F_c = 1 - \left(\frac{\mathrm{NDVI}_{\max} - \mathrm{NDVI}}{\mathrm{NDVI}_{\max} - \mathrm{NDVI}_{\min}}\right)^n, \tag{6}$$

where $\mathrm{NDVI}_{\max}$ and $\mathrm{NDVI}_{\min}$ are NDVI for fully vegetated surfaces and bare soil, respectively. The coefficient n is a function of leaf orientation distribution within the canopy, the value of which typically ranges from 0.6 to 1.25.[32]

For each component, sensible heat flux is calculated from

$$H_c = \rho C_p \frac{T_c - T_a}{r_a^c}, \tag{7}$$

$$H_s = \rho C_p \frac{T_s - T_a}{r_a^a + r_a^s}. \tag{8}$$

As a result, latent heat flux for each component can be obtained from

$$\mathrm{LE}_c = \frac{R_c}{F_c} - \rho C_p \frac{T_c - T_a}{r_a^c}, \tag{9}$$

$$\mathrm{LE}_s = \frac{R_s - G}{1 - F_c} - \rho C_p \frac{T_s - T_a}{r_a^a + r_a^s}, \tag{10}$$

where ρ is air density (kg/m^3); C_p is the specific heat of air at constant pressure (J/kg/K). r_a^a is the aerodynamic resistance to heat transfer between $Z_{\mathrm{om}} + d$ (Z_{om} is the canopy roughness length for momentum transfer and d is zero displacement height) and the reference height (s/m); r_a^c is the aerodynamic resistance to heat transfer between canopy and the reference height (s/m); and r_a^s is the aerodynamic resistance to heat flow in the boundary layer immediately above the soil surface (s/m). All resistance terms can be calculated following Sánchez et al.[26]

2.1.2 *Trapezoidal framework*

To estimate LE_c and LE_s from Eqs. (9) and (10), surface temperatures for soil and canopy are needed. The decomposition of LST into component temperatures in the HTEM is based on interpretation of the fractional vegetation coverage (F_c)–LST space.[23] As shown in Fig. 1, four critical points relating to four extreme conditions define a trapezoid. Point A represents the driest bare soil with the highest surface temperature ($T_{s,\max}$), and point B represents the fully vegetated surface with largest water stress and therefore highest surface temperature ($T_{c,\max}$). As a result, points A and B constitute the warm edge of the trapezoid space. Warm edge AB represents surfaces with largest water stress within the full range of F_c (from 0 to 1), and ET for those surfaces is assumed to be zero. Conversely, points C and D represent fully vegetated and bare soil surfaces without water stress, respectively. Accordingly, segment CD is referred to as the cold edge, and ET on the cold edge is assumed to be equal to the potential ET.

Soil wetness isolines representing constant soil water availability were found existing in the F_c–LST space[33] (Fig. 1). Since radiometric temperature of the soil surface is mostly affected by the soil wetness and soil texture, while the latter remains relatively constant for a certain region, it is reasonable to assume that each soil wetness isoline represents the same soil surface temperature.[24,33] Therefore, soil wetness isolines are used to decompose bulk radiative temperature observed by remote sensing into component temperatures.[23] For example, points E and F in Fig. 1 have the same soil surface temperature. The slope of each isoline is derived by interpolating the slope of the warm edge and that of the cold edge in terms of temperature difference between the pixel and cold edge (a) and that between the pixel and warm edge (b). Soil surface temperature for each pixel can be computed from

$$T_s = F_c \times \frac{a}{a+b}(T_{s,\max} - T_{c,\max}) + \mathrm{LST}, \tag{11}$$

$$a = \mathrm{LST} - T_{\min}, \tag{12}$$

$$b = (1 - F_c)(T_{s,\max} - T_{c,\max}) + T_{c,\max} - \mathrm{LST}, \tag{13}$$

where $T_{\min}$ is surface temperature for the cold edge.

A linear assumption of $\mathrm{LST} = F_c T_c + (1 - F_c) T_s$ is used in HTEM to explain soil moisture isolines.[23] Therefore, canopy surface temperature can be determined from

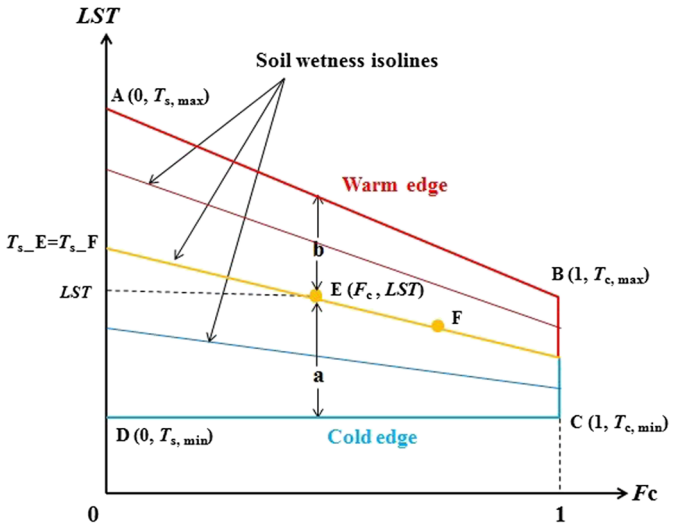

Fig. 1 The trapezoidal framework of the hybrid dual source scheme and trapezoid framework based evapotranspiration model (HTEM) and soil wetness isolines.

$$T_c = \frac{\mathrm{LST} - (1 - F_c)T_s}{F_c}. \tag{14}$$

2.1.3 *Determination of the boundary conditions*

Different from other triangle/trapezoid framework based ET models, the warm and cold edges in HTEM are determined theoretically. This feature makes HTEM avoid the subjectivities and uncertainties in determining these extreme boundaries based on visual interpretation of satellite imagery being used.[34] The explicit expression of T_s can be obtained by combining the surface radiation budget [Eq. (15)] and energy balance [Eq. (16)] equations for the soil component.

$$R_s = (1 - \alpha_s)S_d + \varepsilon_s\varepsilon_a\sigma T_a^4 - \varepsilon_s\sigma T_s^4 \quad \approx (1 - \alpha_s)S_d + \varepsilon_s\varepsilon_a\sigma T_a^4 - \varepsilon_s\sigma T_a^4 - 4\varepsilon_s\sigma T_a^3(T_s - T_a), \tag{15}$$

$$R_s - G = H_s + \mathrm{LE}_s = \rho C_p\left(\frac{T_s - T_a}{r_a^a + r_a^s}\right) + \mathrm{LE}_s, \tag{16}$$

where α_s is the albedo for the soil component and ε_s is the broadband emissivity of the soil surface.

Substituting Eq. (15) into Eq. (16), we get

$$T_s = \frac{(1 - \alpha_s)S_d + \varepsilon_s\varepsilon_a\sigma T_a^4 - \varepsilon_s\sigma T_a^4 - \mathrm{LE}_s/(1 - G/R_s)}{4\varepsilon_s\sigma T_a^3 + \rho C_p/[(r_a^a + r_a^s)(1 - G/R_s)]} + T_a. \tag{17}$$

For theoretical driest bare surface (point A), $T_{s,\max}$ can be obtained by letting $\mathrm{LE}_s = 0$ in Eq. (17). The ground heat flux (G) in HTEM is taken to be a constant ratio of R_s (i.e., $G = c \times R_s$). Therefore,

$$T_{s,\max} = \frac{(1 - \alpha_s)S_d + \varepsilon_s\varepsilon_a\sigma T_a^4 - \varepsilon_s\sigma T_a^4}{4\varepsilon_s\sigma T_a^3 + \rho C_p/[(r_a^a + r_a^s)(1 - c)]} + T_a. \tag{18}$$

Similarly, for vegetation component, canopy surface temperature can be expressed as

$$T_c = \frac{(1 - \alpha_c)S_d + \varepsilon_c\varepsilon_a\sigma T_a^4 - \varepsilon_c\sigma T_a^4 - \mathrm{LE}_c}{4\varepsilon_c\sigma T_a^3 + \rho C_p/r_a^c} + T_a, \tag{19}$$

where α_c is the albedo for the canopy component; and ε_c is the canopy surface emissivity.

Let $\mathrm{LE}_c = 0$ in Eq. (19); $T_{c,\max}$ can be expressed as

$$T_{c,\max} = \frac{(1 - \alpha_c)S_d + \varepsilon_c\varepsilon_a\sigma T_a^4 - \varepsilon_c\sigma T_a^4}{4\varepsilon_c\sigma T_a^3 + \rho C_p/r_a^c} + T_a. \tag{20}$$

For the cold edge, the largest evaporation rate corresponds to the lowest sensible heat flux. Therefore, spatially averaged air temperature (T_a) is taken to be the horizontal cold edge.[34] It should be noticed that the advection effect is not considered in the HTEM.

2.2 *Upscaling Instantaneous ET into Daily Value*

Since satellite remote sensing could only provide land surface information at satellite overpass time, it is necessary to upscale these instantaneous ET ($\mathrm{ET}_{\mathrm{inst}}$) values into daily values. In HTEM, it is assumed that the reference evaporative fraction (F_{ET}) is a constant throughout a day.[35]

$$F_{\mathrm{ET}} = \frac{\mathrm{ET}_{\mathrm{inst}}}{\mathrm{ET}_{r\mathrm{inst}}}, \tag{21}$$

where $\mathrm{ET}_{r\mathrm{inst}}$ is the reference ET at satellite image time, which can be calculated using the Penman-Monteith method recommended by Food and Agriculture Organization (FAO).[31]

Daily ET ($\mathrm{ET}_{\mathrm{day}}$) is then computed as

$$\mathrm{ET}_{\mathrm{day}} = F_{\mathrm{ET}} \times \mathrm{ET}_{r\mathrm{day}}, \tag{22}$$

where $\mathrm{ET}_{r\_\mathrm{day}}$ is the cumulative 24 h ET_r for the day of the image.

To obtain daily E and T, it is further assumed that the ratio of T to ET is a constant within a day when precipitation in that day is negligible (i.e., <2 mm). This assumption is reasonable as the partitioning of E and T is mostly affected by vegetation conditions and soil water status, which keep relative constant for short time period (e.g., day or subdays).[36]

3 Study Site and Data

3.1 *Site Description*

The data to validate the model comes from the Lucky Hills study site on the U.S. Department of Agriculture-Agricultural Research Service (USDA-ARS) Walnut Gulch Experimental Watershed in southeastern Arizona (110.051°W, 31.744°N). The elevation of the site ranges from 1363 to 1375 m. Mean annual temperature is 17°C and mean annual rainfall (1970 to 1999) is 322 mm, with approximately two thirds of it occurring in the monsoon season (July to September).[8] The soils are mainly sandy loam with a high fraction of fragmented rocks.[37] The vegetation on the Lucky Hills watershed is a shrub-dominated ecosystem with creosotebush (*Larrea tridentate*), mariola (*Partheniumincanum*), whitethorn acacia (*Acacia constricta*), littleleaf sumac (*Rhusmicrophylla*), and tarbush (*Flourensiacernua*).[8] The shrubs average ~0.6 m high and cover ~26% of the land surface.[37] Detailed descriptions of the site can be found in Emmerich,[38] Scott et al.,[8] and Scott et al.[39]

3.2 *Measurements and Data*

During the growing season of 2003 day of the year [(DOY) 185 to 328], comprehensive experiments were conducted in the Lucky Hills site.[8] Briefly, meteorological data including air temperature, humidity, wind speed, net radiation, and precipitation were recorded by a weather station at the experimental site. Volumetric soil water content at soil profile up to 2 m depth was measured with time-domain reflectometry. Sensible and latent heat fluxes over the bulk surface were measured using a Bowen-ratio system at 20-min interval with a fetch of over 1 km in all directions. Shrub transpiration was measured using the constant heat balance sap-flow meter[40] set on 16 individual stems at 30-min interval and stem-level water use was scaled to ecosystem transpiration (T). The values of ET and T in a 24-h period were summed to give daily values. As a result, daily soil evaporation (E) was estimated by subtracting daily T from daily ET. In addition, during DOY 203 to 288, soil and canopy radiometric temperatures were measured simultaneously with infrared radiometers. Parameters of the HTEM used in this study are included in Table 1.

3.3 *Satellite Images*

Moderate resolution imaging spectroradiometer (MODIS) data were used in this study because of its high temporal resolution (1 to 2 days) and accessible spatial resolution (250 to 1000 m). Three derived MODIS land surface products were downloaded from NASA's Data and Information System (http://reverb.echo.nasa.gov). LST and surface emissivity were acquired from the daily LST and emissivity product (MOD11A1, 1000 m), and narrow band spectral reflectances were obtained from the daily surface reflectance product (MOD09GA, 1000 m). LAI was acquired from the eight-day LAI products (MOD15A2, 1000 m), and linear interpolation between two bounding observations was used to obtain the daily LAI value. Liang's

Table 1 Parameters used in the study.

Parameter	Symbol	Value	Source
Albedo for soil surface	α_s	0.13	41
Albedo for canopy surface	α_c	0.24	41
Soil surface emissivity	ε_s	0.96	26
Canopy surface emissivity	ε_c	0.985	26
Coefficient in Eq. (14)	n	0.80	Site specified
Maximum normalized difference vegetation index (NDVI)	$NDVI_{max}$	0.89	32
Minimum NDVI	$NDVI_{min}$	0.10	32
Radiation extinction coefficient	k_c	0.40	29
Ratio of G to R_n	c	0.35	23

method[42] was used to calculate broadband surface reflectance from seven short-wave channels, and NDVI was derived from red and near-infrared bands following Huete et al.[43] During the experiment period, 94 MODIS images were available for the Lucky Hills site, 58 of which are between DOY 203 to DOY 288.

4 Results and Discussion

4.1 *Temperature Variables*

Figure 2 shows trends in observed air temperature (T_a) and estimated surface temperatures for the two extreme conditions (driest bare soil surface and driest fully vegetated surface) at satellite overpass time during the study period. Temperatures for the fully vegetated surface with largest water stress ($T_{c,\max}$) are systematically lower than those for extreme dry bare soil ($T_{s,\max}$) but higher than the corresponding air temperature. This demonstrates the validity of the trapezoidal framework, but not the triangle method[18,32] or rectangular method,[44–46] because the triangle method assumes an identical $T_{c,\max}$ and $T_{c,\min}$ and the rectangular method assumes a same $T_{c,\max}$ and $T_{s,\max}$. For the whole period, the three variables show a similar declining trend from summer to winter. However, the variation ranges of $T_{c,\max}$ and $T_{s,\max}$ are obviously larger than that of T_a. This is because $T_{c,\max}$ and $T_{s,\max}$ are determined not only by T_a but also by radiation and surface aerodynamic characteristics. Interestingly, the variation trends in $T_{c,\max}$ and $T_{s,\max}$ are very similar. This is likely due to the relative small variations in vegetation coverage and leaf area during the study period.

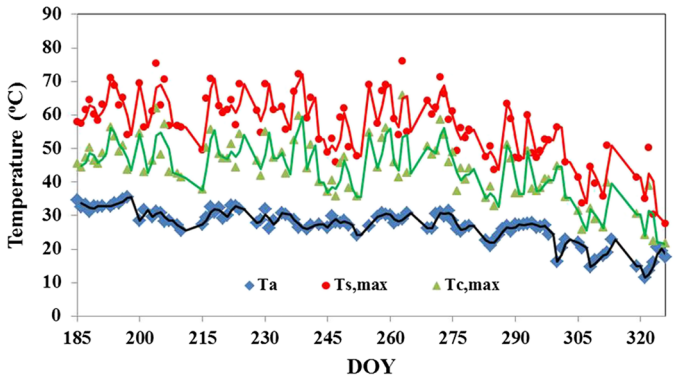

Fig. 2 Trends of T_a, $T_{s,\max}$, and $T_{c,\max}$ at daily satellite passing time during the study period. Solid lines are three-day moving average results for each variable.

Figure 3 shows the comparison between observed component temperatures (T_s and T_c) and those estimated by HTEM. Overall, the HTEM performed reasonably well in decomposing the bulk radiative temperature from MODIS into component temperatures, thus showing a root-mean-square error (RMSE) of 1.77°C for T_s and 2.25°C for T_c. This result is similar to other published studies on temperature decomposition with ground-based multiangle thermal infraRed (TIR) measurements. Based on *in situ* TIR measurements, Kimes[47] reported an RMSE of 1°C for the vegetation temperature and 2°C for the soil temperature with respect to observed component temperatures. Similar errors were obtained by Merlin and Chehbouni.[48] Generally, the decomposing errors range between 1 and 2°C. However, considering the measurement errors by MODIS sensor (±1°C, Wan et al.[49]), the current results seem satisfactory.

Comparisons between surface energy balance components (R_n, G, H, and LE) produced by HTEM with MODIS data and those from the Bowen-ratio system are shown in Fig. 4. All fluxes and meteorological measurements were linearly interpolated to the time of satellite overpass using the two adjacent bounding values.

It is encouraging to see that all four energy components estimated from HTEM agree well with Bowen-ratio observations. Estimated R_n has an RMSE of 22.3 W/m^2 and a mean bias (defined as mean estimated values minus mean observed value) of 3.7 W/m^2 [Fig. 4(a)]. For G estimation, a constant value of $c = 0.35$ was used, corresponding to the midpoint between its likely limits.[50] A similar value was also used in Li et al.[32] and Sánchez et al.[26] The simulated G

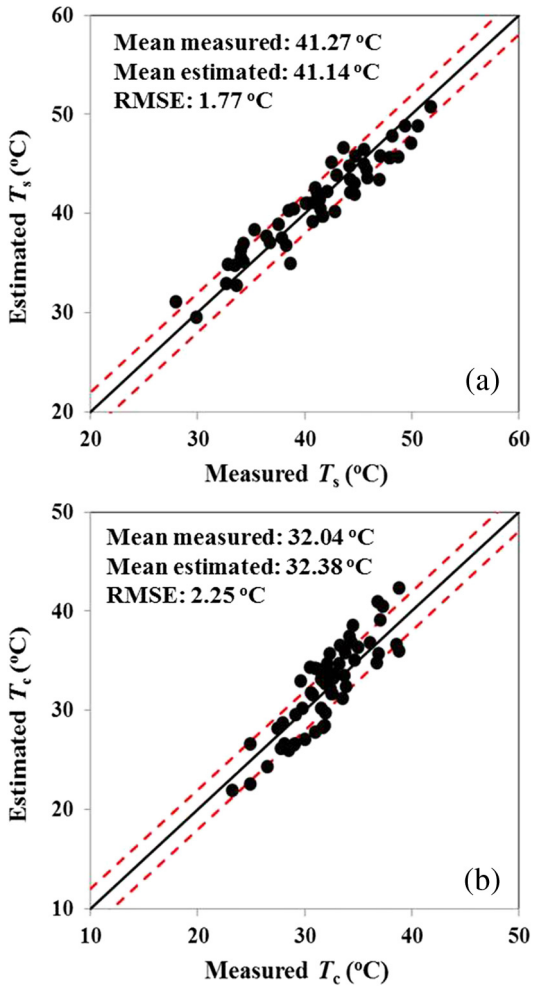

Fig. 3 Comparisons between measured component temperatures and those estimated from the HTEM. (a) Soil surface temperature. (b) Canopy surface temperature. Dashed lines represent ±2°C boundaries.

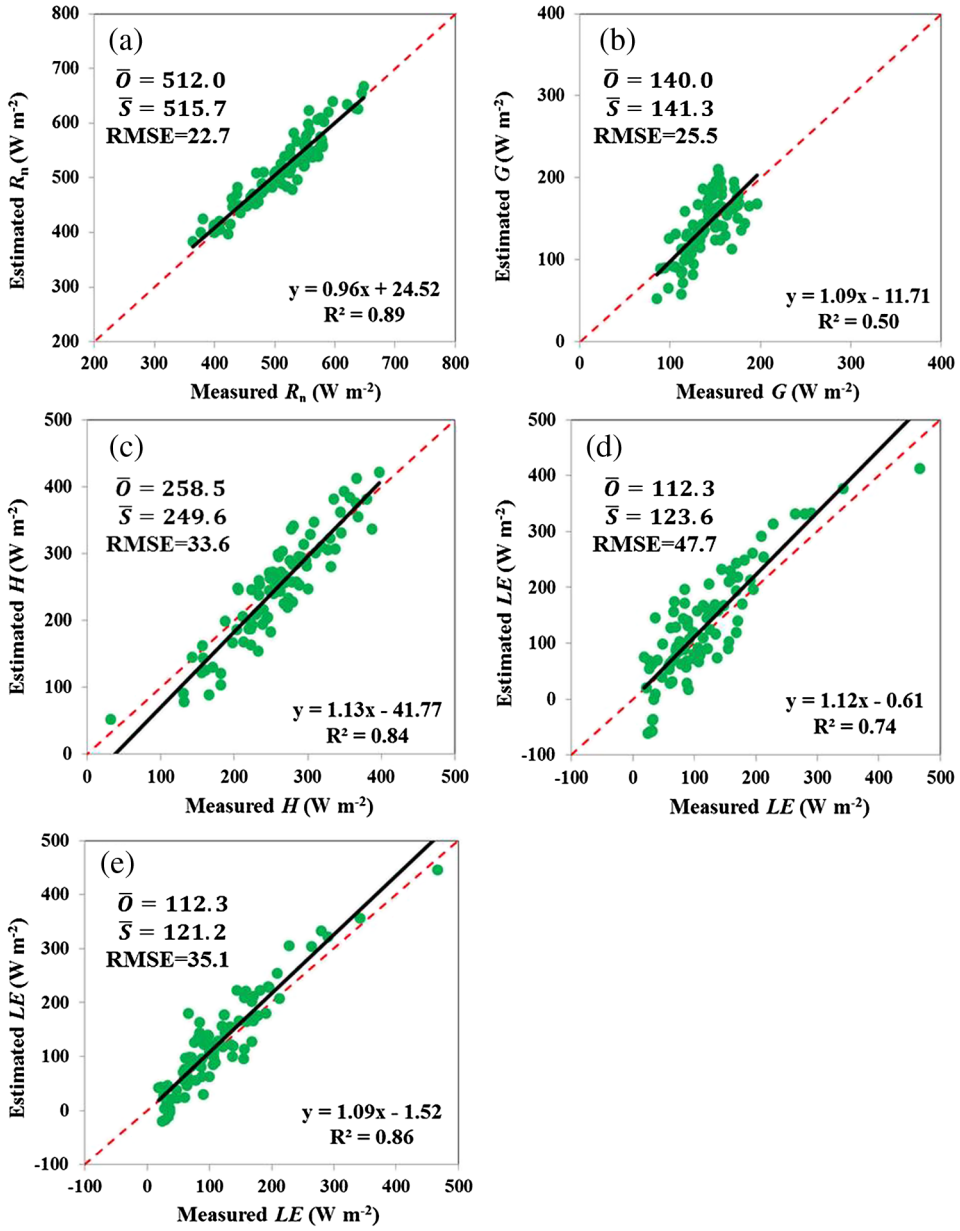

Fig. 4 Comparisons between measured and estimated energy flux components (a) R_n, (b) G, (c) H, (d) LE, and (e) LE estimated with observed R_n and G. $\bar{O}$ is mean observed values, $\bar{S}$ is mean estimated values, and RMSE is the root mean square error (W/m^2).

overestimated observation by 1.3 W/m^2 on average, with an RMSE of 25.5 W/m^2 [Fig. 4(b)]. A local calibration of coefficient c would likely improve the model performance in G estimation, which, however, is not the major concern of this study.

The HTEM reproduces observed H fairly well, with RMSE = 33.6 W/m^2 and mean bias = −8.9 W/m^2 [Fig. 4(c)]. However, there is a small tendency to overestimate H at high H and underestimate H at low H. For LE obtained by HTEM, RMES = 47.7 W/m^2 and mean bias = 11.3 W/m^2 with reference to Bowen-ratio observations [Fig. 4(d)]. This relatively larger error of LE is due in part to errors in R_n and G estimates, as LE is calculated to be a residual term in the surface energy balance equation. To minimize uncertainties in R_n and G, measured R_n and G were applied in Eqs. (9) and (10) to calculate LE [Fig. 4(e)]. Not surprisingly, R^2 between estimated LE and observed LE increases to 0.86, and RMSE = 35.1 W/m^2 and mean bias = 8.9 W/m^2. This suggests the potential to improve LE estimation by improving the accuracy of R_n and G estimated from remote sensing data.

4.2 *ET, E, and T*

Comparison between observed and estimated daily ET from HTEM is shown in Fig. 5, and comparisons between observed E and T partitioning and those by HTEM are shown in Fig. 6. To accommodate the assumption that daily T/ET is a constant, days with precipitation >2 mm were excluded in this analysis. As a result, 74 days remain in the following validation. The reason to validate E and T partitioning at only daily level is that instantaneous sap flow might not equal the transpiration at any given time due to the lag between transpiration and sap flow and the change of stem storage.[51] Also, observed R_n and G were used to minimize uncertainties in these two variables.

For daily ET, agreement between estimates and observations is generally good within the whole growing season (Fig. 5). However, during the two distinct dry-down periods (DOY 255 to 263 and DOY 280 to 305), the modeling errors of ET are obviously larger than those in other periods. This could be partly attributed to the modeling errors in component temperatures. With the surface drying down, the temperature difference between the two components would increase, which may lead to higher absolute error in decomposing the bulk radiative temperature into component temperatures (larger errors were found in the high end of both T_s and T_c, as shown in Fig. 2). The process of ET is strongly coupled to precipitation in this site, which is a typical phenomenon in water-limited ecosystems.[15,52,53] Although over half of simulated results are greater than measured values, the RMSE is only 0.52 mm/day. The mean bias between estimated daily ET and observed value is 0.31 mm/day.

For E and T partitioning, both simulated daily E and T are in good agreement with observations (Fig. 6). The RMSE of estimated E and T are 0.36 and 0.41 mm/day with respect to measurements, respectively. These uncertainties may be attributed to the incomplete description of land surface processes in the model, but could also likely result from errors in MODIS inputs and ground observations. For example, the eight-day composite LAI data of MODIS may not reflect the actual LAI conditions of the day being studied, especially during the greening and senescence periods.[54] Studies have shown that there are great difficulties in upscaling the plant sap-flow measurements into stand transpiration.[55,56] Meanwhile, the assumption of a constant daily T/ET may result in uncertainties as well. Based on measurements, Yang et al.[57] showed that soil water potential declined gradually within rain-free days. This declined trend in soil moisture may be very small for the root zone but can be fairly large for soil surface. This may explain why E estimates show a relative larger error than T. However, as MODIS Terra data provide daily information around noon time, T/ET estimated at overpass time may reflect an average T/ET condition for the entire day. Similar to total ET, both E and T follow the dynamics of precipitation processes. Evaporation peaked on either the day of or the day after the rain pulse and rapidly declined in the following days. This is mainly due to the large drying power of the air and poor surface soil water retention capability in the site. However, transpiration declined

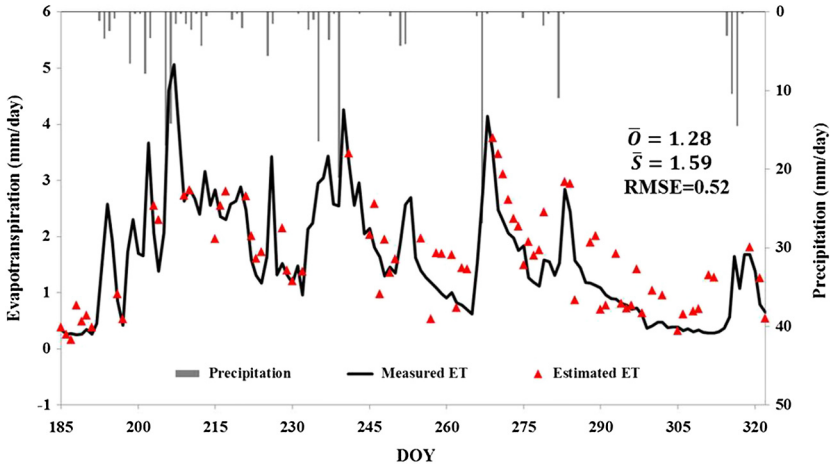

Fig. 5 Comparison between observed and estimated daily evapotranspiration during the study period. $\bar{O}$ is mean observed values, $\bar{S}$ is mean estimated values, and RMSE is the root mean square error (mm/day).

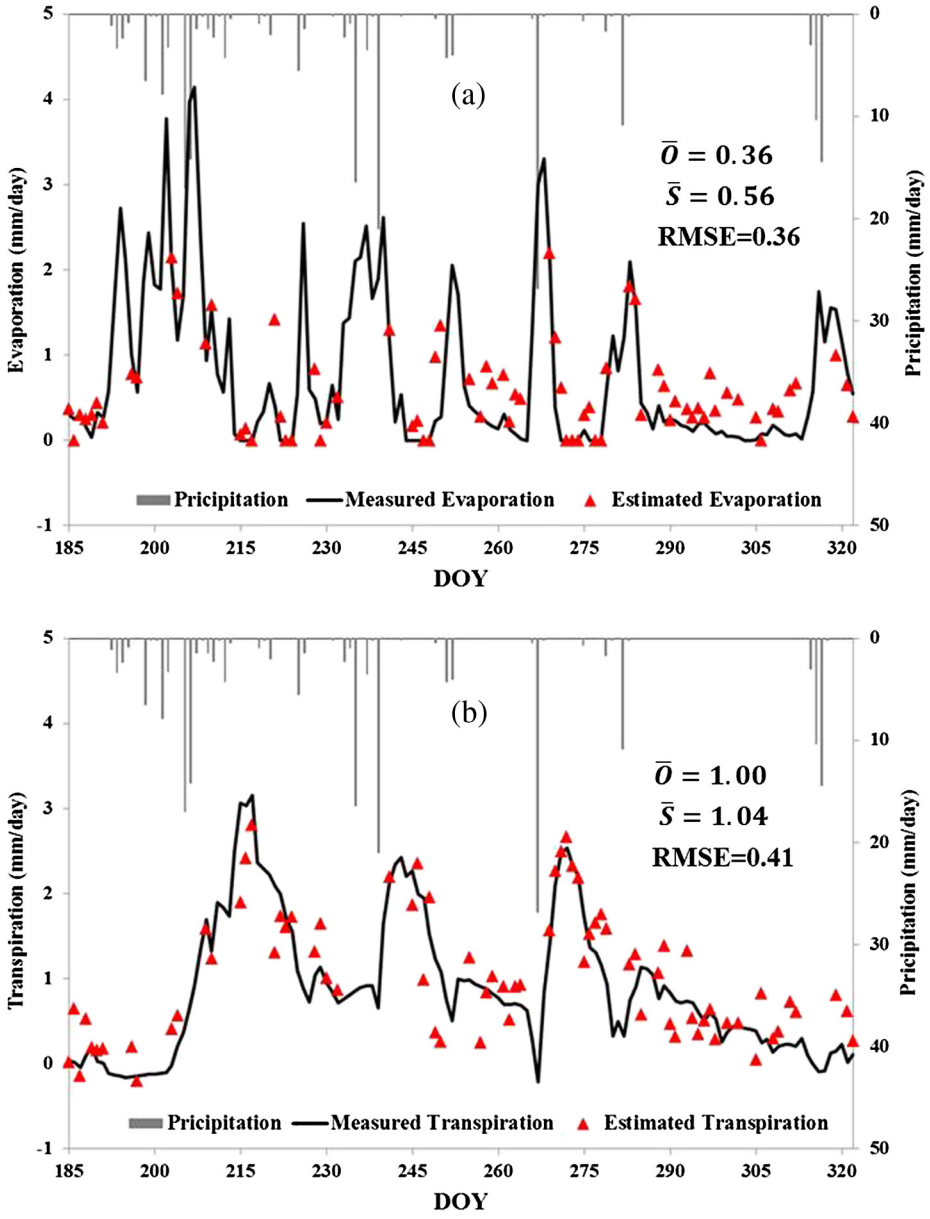

Fig. 6 Comparison between observed and estimated daily (a) evaporation and (b) transpiration during the study period. $\bar{O}$ is mean observed values, $\bar{S}$ is mean estimated values, and RMSE is the root mean square error (mm/day).

more gradually after rainfall events, indicating larger water retention capacity of the root zone and greater resistance in the transpiration pathway that have developed from dry antecedent conditions.[58]

5 Conclusions

In this study, HTEM was applied to estimate surface energy fluxes and evapotranspiration partitioning over a semiarid shrub ecosystem from MODIS images. The results indicate that the following:

1. The HTEM capably decomposes remotely sensed bulk surface radiative temperature into component temperatures, with an RMSE of 1.77°C for soil and 2.25°C for canopy.
2. Validation of the HTEM, using measurements of surface energy fluxes at satellite overpass time, yields RMSE ranging from 22.3 to 47.7 W/m^2 for R_n, G, H, and LE.

Significantly higher agreement was obtained between LE estimates and measurements when observed R_n and G were used (RMSE: 35.1 W/m^2 versus 47.7 W/m^2).

3. With reference to Bowen-ratio and sap-flow measurements, the RMSEs of estimated daily ET, E, and T are 0.52, 0.36, and 0.41 mm/day, respectively, indicating reasonable performance of the HTEM in estimating daily E and T partitioning. However, further efforts are needed, particularly to assess the upscaling method of instantaneous E and T into values at daily or for longer timescales.

Acknowledgments

This work is financially supported by Australian National Center for Groundwater Research and Training, the National Natural Science Foundation of China (Grant No. 51279077), and the National Key Technology R&D Program of China (Grant No. 2011BAD25B05).

References

1. A. Parsons and A. Abrahams, *Geomorphology of Desert Environments*, pp. 1–12, CRC Press, Boca Raton, Florida (1994).
2. B. D. Newman et al., "Ecohydrology of water-limited environments: a scientific vision," *Water Resour. Res.* **42**(6), W06302 (2006), http://dx.doi.org/10.1029/2005WR004141.
3. I. Rodriguez-Iturbe and A. Porporato, *Ecohydrology of Water-Controlled Ecosystems*, Cambridge University Press, New York (2004).
4. J. H. C. Cornelissen et al., "Global negative vegetation feedback to climate warming responses of leaf litter decomposition rates in cold biomes," *Ecol. Lett.* **10**(7), 619–627 (2007), http://dx.doi.org/10.1111/j.1461-0248.2007.01051.x.
5. T. E. Huxman et al., "Ecohydrological implication of wood plant encroachment," *Ecology* **86**(2), 308–319 (2005), http://dx.doi.org/10.1890/03-0583.
6. N. Zeng et al., "Enhancement of interdecadal climate variability in the Sahel by vegetation interaction," *Science* **286**(5444), 1537–1540 (1999), http://dx.doi.org/10.1126/science.286.5444.1537.
7. J. F. Reynolds et al., "Effects of long-term rainfall variability on evapotranspiration and soil water distribution in the Chihuahuan Desert: a modeling analysis," *Plant Ecol.* **150**(1), 145–159 (2000), http://dx.doi.org/10.1023/A:1026530522612.
8. R. L. Scott et al., "Partitioning of evapotranspiration and its relation to carbon dioxide exchange in a Chihuahuan Desert shrubland," *Hydrol. Process.* **20**(15), 3227–3243 (2006), http://dx.doi.org/10.1002/(ISSN)1099-1085.
9. D. D. Baldocchi, "Assessing the eddy covariance technique for evaluating carbon dioxide exchange rates of ecosystems: past, present and future," *Glob. Change Biol.* **9**(4), 479–492 (2003), http://dx.doi.org/10.1046/j.1365-2486.2003.00629.x.
10. P. González-Altozano et al., "Comparative assessment of five methods of determining sap flow in peach trees," *Agric. Water Manage.* **95**(5), 503–515 (2008), http://dx.doi.org/10.1016/j.agwat.2007.11.008.
11. M. S. Moran et al., "Partitioning evapotranspiration in semiarid grassland and shrubland ecosystems using time series of soil surface temperature," *Agric. Forest Meteorol.* **149**, 59–72 (2009), http://dx.doi.org/10.1016/j.agrformet.2008.07.004.
12. E. A. Yepez et al., "Partitioning overstory and understory evapotranspiration in a semiarid savanna woodland form the isotopic composition of water vapor," *Agric. Forest Meteorol.* **119**(1–2), 43–68 (2003), http://dx.doi.org/10.1016/S0168-1923(03)00116-3.
13. F. Domingo et al., "Evapotranspiration model for semi-arid shrub-lands tested against data from SE Spain," *Agric. Forest Meteorol.* **95**(2), 67–84 (1999), http://dx.doi.org/10.1016/S0168-1923(99)00031-3.
14. P. Gowda et al., "ET mapping for agricultural water management: present status and challenges," *Irrig. Sci.* **26**(3), 223–237 (2008), http://dx.doi.org/10.1007/s00271-007-0088-6.
15. Y. T. Yang et al., "Remote sensing temporal and spatial patterns of evapotranspiration and the responses to water management in a large irrigation district of North China," *Agric. Forest Meteorol.* **164**, 112–122 (2012), http://dx.doi.org/10.1016/j.agrformet.2012.05.011.

16. K. W. Brown and N. J. Rosenberg, "A resistance model to predict evapotranspiration and its application to a sugar beet field," *Agron. J.* **65**(3), 341–347 (1973), http://dx.doi.org/10.2134/agronj1973.00021962006500030001x.
17. W. G. M. Bastiaanssen et al., "A remote sensing surface energy balance algorithm for land (SEBAL)-1. Formulation," *J. Hydrol.* **213**(1–4), 198–212 (1998), http://dx.doi.org/10.1016/S0022-1694(98)00253-4.
18. L. Jiang and S. Islam, "A methodology for estimation of surface evapotranspiration over large areas using remote sensing observations," *Geophys. Res. Lett.* **26**(17), 2773–2776 (1999), http://dx.doi.org/10.1029/1999GL006049.
19. Z. Su, "The surface energy balance system (SEBS) for estimation of turbulent heat fluxes," *Hydrol. Earth Syst. Sci.* **6**(1), 85–99 (2002), http://dx.doi.org/10.5194/hess-6-85-2002.
20. A. Verhoef et al., "Some practical notes on the parameter kB–1 for sparse vegetation." *J. Appl. Meteorol.* **36**(5), 560–572 (1997), http://dx.doi.org/10.1175/1520-0450(1997)036<0560:SPNOTP>2.0.CO;2.
21. Y. T. Yang et al., "Development of a soil-plant-atmosphere continuum model (HDS-SPAC) based on hybrid dual-source approach and its verification in wheat field," *Sci. China Technol. Sci.* **55**(10), 1–15 (2012).
22. W. P. Kustas and J. M. Norman, "A two-source approach for estimating turbulent fluxes using multiple angle thermal infrared observations," *Water Resour. Res.* **33**(6), 1495–1508 (1997), http://dx.doi.org/10.1029/97WR00704.
23. D. Long and V. P. Singh, "A two-source trapezoid model for evapotranspiration (TTME) from satellite imagery," *Remote Sens. Environ.* **121**(0), 370–388 (2012), http://dx.doi.org/10.1016/j.rse.2012.02.015.
24. K. Nishida et al., "An operational remote sensing algorithm of land surface evaporation," *J. Geophys. Res.* **108**(D9), 4270 (2003), http://dx.doi.org/10.1029/2002JD002062.
25. J. M. Norman et al., "Source approach for estimating soil and vegetation energy fluxes in observations of directional radiometric surface temperature," *Agric. Forest Meteorol.* **77**(3–4), 263–293 (1995), http://dx.doi.org/10.1016/0168-1923(95)02265-Y.
26. J. M. Sánchez et al., "Modeling surface energy fluxes over maize using a two-source patch model and radiometric soil and canopy temperature observations," *Remote Sens. Environ.* **112**(3), 1130–1143 (2008), http://dx.doi.org/10.1016/j.rse.2007.07.018.
27. Y. T. Yang and S. H. Shang, "A hybrid dual source scheme and trapezoid framework-based evapotranspiration model (HTEM) using satellite images: algorithm and model test," *J. Geophys. Res.* **118**(5), 2284–2300 (2013), http://dx.doi.org/10.1002/jgrd.50259.
28. N. Agam et al., "Application of the Priestley–Taylor approach in a two-source surface energy balance model," *J. Hydrometeorol.* **11**(1), 185–198 (2010), http://dx.doi.org/10.1175/2009JHM1124.1.
29. H. D. Guan and J. Wilson, "A hybrid dual-source model for potential evaporation and transpiration partitioning," *J. Hydrol.* **377**(3–4), 405–416 (2009), http://dx.doi.org/10.1016/j.jhydrol.2009.08.037.
30. W. Brutsaert, "On a derivable formula for long-wave radiation from clear skies," *Water Resour. Res.* **11**(5), 742–744 (1975), http://dx.doi.org/10.1029/WR011i005p00742.
31. R. G. Allen et al., "Crop evapotranspiration: guidelines for computing crop water requirements," *FAO Irrigation and Drainage Paper 56*, pp. 300, Rome (1998).
32. F. Li et al., "Utility of remote sensing–based two-source energy balance model under low- and high-vegetation cover conditions," *J. Hydrometeorol.* **6**(6), 878–891 (2005), http://dx.doi.org/10.1175/JHM464.1.
33. T. Carlson, "An overview of the 'triangle method' for estimating surface evapotranspiration and soil moisture from satellite imagery," *Sensors* **7**(8), 1612–1629 (2007), http://dx.doi.org/10.3390/s7081612.
34. D. Long et al., "Deriving theoretical boundaries to address scale dependencies of triangle models for evapotranspiration estimation," *J. Geophys. Res.* **117**(D5), D05113 (2012), http://dx.doi.org/10.1029/2011JD017079.
35. R. G. Allen et al., "Satellite-based energy balance for mapping evapotranspiration with internalized calibration (METRIC)-model," *J. Irrig. Drain. Eng.* **133**, 380–394 (2007), http://dx.doi.org/10.1061/(ASCE)0733-9437(2007)133:4(380).

36. P. Gentine et al., "The diurnal behavior of evaporative fraction in the soil-vegetation-atmospheric boundary later continuum," *J. Hydrometeorol.* **12**, 1530–1546 (2011), http://dx.doi.org/10.1175/2011JHM1261.1.
37. J. C. Ritchie et al., "Patterns of soil erosion and redeposition on Lucky Hills Watershed, Walnut Gulch Experimental Watershed, Arizona," *Catena* **61**(2–3), 122–130 (2005), http://dx.doi.org/10.1016/j.catena.2005.03.012.
38. W. E. Emmerich, "Carbon dioxide fluxes in a semiarid environment with high carbonate soils," *Agric. Forest Meteorol.* **116**(1–2), 91–102 (2003), http://dx.doi.org/10.1016/S0168-1923(02)00231-9.
39. R. L. Scott et al., "Modeling multiyear observations of soil moisture recharge in the semiarid American Southwest," *Water Resour. Res.* **36**(8), 2233–2247 (2000), http://dx.doi.org/10.1029/2000WR900116.
40. J. F. Kjelgaard et al., "Measuring sap flow with the heat balance approach using constant and variable heat inputs," *Agric. Forest Meteorol.* **85**(3–4), 239–250 (1997), http://dx.doi.org/10.1016/S0168-1923(96)02397-0.
41. G. S. Campbell and J. M. Norman, *An Introduction to Environmental Biophysics*, Springer, New York (1998).
42. S. Liang, "Narrowband to broadband conversions of land surface albedo I: algorithms," *Remote Sens. Environ.* **76**(2), 213–238 (2001), http://dx.doi.org/10.1016/S0034-4257(00)00205-4.
43. A. Huete et al., "Overview of the radiometric and biophysical performance of the MODIS vegetation indices," *Remote Sens. Environ.* **83**(1–2), 195–213 (2002), http://dx.doi.org/10.1016/S0034-4257(02)00096-2.
44. N. Batra et al., "Estimation and comparison of evapotranspiration from MODIS and AVHRR sensors for clear sky days over the Southern Great Plains," *Remote Sens. Environ.* **103**(1), 1–15 (2006), http://dx.doi.org/10.1016/j.rse.2006.02.019.
45. L. Jiang et al., "A satellite-based daily actual evapotranspiration estimation algorithm over South Florida," *Glob. Planet. Change* **67**(1–2), 62–77 (2009), http://dx.doi.org/10.1016/j.gloplacha.2008.12.008.
46. D. Long and V. P. Singh, "Assessing the impact of end-member selection on the accuracy of satellite-based spatial variability models for actual evapotranspiration estimation," *Water Resour. Res.* **49**(5), 2601–2618 (2013), http://dx.doi.org/10.1002/wrcr.v49.5.
47. D. S. Kimes, "Remote sensing of row crop structure and component temperatures using directional radiometric temperatures and inversion techniques," *Remote Sens. Environ.* **13**(1), 33–55 (1983), http://dx.doi.org/10.1016/0034-4257(83)90026-3.
48. O. Merlin and A. Chehbouni, "Different approaches in estimating heat flux using dual angle observations of radiative surface temperature," *Int. J. Remote Sens.* **25**(1), 275–289 (2004), http://dx.doi.org/10.1080/0143116031000116408.
49. Z. Wan et al., "Validation of the land-surface temperature products retrieved from terra moderate resolution imaging spectroradiometer data," *Remote Sens. Environ.* **83**(1–2), 163–180 (2002), http://dx.doi.org/10.1016/S0034-4257(02)00093-7.
50. B. J. Choudhury et al., "Analysis of an empirical model for soil heat flux under a growing wheat crop for estimating evaporation by an infrared-temperature based energy balance equation," *Agric. Forest Meteorol.* **39**(4), 283–297 (1987), http://dx.doi.org/10.1016/0168-1923(87)90021-9.
51. J. Čermák et al., "Tree water storage and its diurnal dynamics related to sap flow and changes in stem volume in old-growth Douglas-fir trees," *Tree Physiol.* **27**(2), 181–198 (2007), http://dx.doi.org/10.1093/treephys/27.2.181.
52. P. Mielnick et al., "Long-term measurements of CO2 flux and evapotranspiration in a Chihuahuan desert grassland," *J. Arid Environ.* **60**(3), 423–436 (2005), http://dx.doi.org/10.1016/j.jaridenv.2004.06.001.
53. H. E. Unland et al., "Surface flux measurement and modeling at a semi-arid Sonoran Desert site," *Agric. Forest Meteorol.* **82**(1–4), 119–153 (1996), http://dx.doi.org/10.1016/0168-1923(96)02330-1.
54. N. Guindin-Garcia et al., "An evaluation of MODIS 8- and 16-day composite products for monitoring maize green leaf area index," *Agric. Forest Meteorol.* **161**, 15–25 (2012), http://dx.doi.org/10.1016/j.agrformet.2012.03.012.

55. W. Trambouze et al., "Comparison of methods for estimating actual evapotranspiration in a row-cropped vineyard," *Agric. Forest Meteorol.* **91**(3–4), 193–208 (1998), http://dx.doi.org/10.1016/S0168-1923(98)00072-0.
56. Y. Q. Zhang et al., "Evapotranspiration components determined by sap flow and micro-lysimetry techniques of a vineyard in northwest China: dynamics and influential factors," *Agric. Water Manage.* **98**(8), 1207–1214 (2011), http://dx.doi.org/10.1016/j.agwat.2011.03.006.
57. Y. T. Yang et al., "Examination and parameterization of the root water uptake model from stem water potential and sap flow measurements," *Hydrol. Process.* **27**(20), 2857–2863 (2013).http://dx.doi.org/10.1002/hyp.9406
58. W. J. Shuttleworth and J. S. Wallace, "Evaporation from sparse crops—an energy combination theory," *Q. J. R. Meteorol. Soc.* **111**(469), 839–855 (1985), http://dx.doi.org/10.1002/qj.49711146910.